European Journal of Pharmacology 960 (2023) 176138

Contents lists available at ScienceDirect

European Journal of Pharmacology

journal homepage: www.elsevier.com/locate/ejphar

The pro-healing effects of heparan sulfate and growth factors are enhanced by the heparinase enzyme: New association for skin wound healing treatment

Raffaella Belvedere [a,**], Nunzia Novizio [a], Mariangela Palazzo [a], Emanuela Pessolano [b], Antonello Petrella [a,*]

[a] Department of Pharmacy, University of Salerno, Fisciano, SA, Italy
[b] Department of Pharmacological Sciences, University of Piemonte Orientale, Novara, Italy

ARTICLE INFO

Keywords:
Skin wound healing
Heparan sulfate
Growth factors
Heparinase
Tissue repair

ABSTRACT

Effective treatment strategies for skin wound repair are the focus of numerous studies. New pharmacological approaches appear necessary to guarantee a correct and healthy tissue regeneration. For these reasons, we purposed to investigate the effects of the combination between heparan sulfate and growth factors further adding the heparinase enzyme. Interestingly, for the first time, we have found that this whole association retains a marked pro-healing activity when topically administered to the wound. In detail, this combination significantly enhances the motility and activation of the main cell populations involved in tissue regeneration (keratinocytes, fibroblasts and endothelial cells), compared with single agents administered without heparinase. Notably, using an experimental C57BL/6 mouse model of skin wounding, we observed that the topical treatment of skin lesions with heparan sulfate + growth factors + heparinase promotes the highest closure of wounds compared to each substance mixed with the other ones in all the possible combinations. Eosin/hematoxylin staining of skin biopsies revealed that treatment with the whole combination allows the formation of a well-structured matrix with numerous new vessels. Confocal analyses for vimentin, FAP1α, CK10 and CD31 have highlighted the presence of activated fibroblasts, differentiated keratinocytes and endothelial cells at the closed region of wounds. Our results encourage defining this combined treatment as a new and appealing therapy expedient in skin wound healing, as it is able to activate cell components and promote a dynamic lesions closure.

1. Introduction

Wound healing is a complex process influenced by different factors including growth factors (GFs) which influence inflammatory responses, epithelialization, granulation tissue formation, and angiogenesis (Han and Ceilley, 2017). Among them, Vascular Endothelial Growth Factor (VEGF), Epithelial Growth Factor (EGF), basic-Fibroblasts Growth Factor (bFGF) are essential for successful matrix formation and remodelling processes in the normal wound healing, while their deficiencies have been reported in chronic pressure ulcers (H. Park et al., 2017).

Skin wound healing is also influenced by resident/invading cells and extracellular matrix components (ECM). Glycosaminoglycans (GAGs) are known as ligands for other ECM macromolecules and interacting with cytokines, chemokines or GFs. Moreover, since GAGs are biocompatible, low immunogenic, biodegradable and resorbable, they are considered ideal candidates as components of wound dressings (Anderegg et al., 2021; Belvedere et al., 2018a,b; Franco et al., 2019, 2020; Petrella et al., 2020). Among GAGs, heparan sulfate (HS) has been recognized important in angiogenesis, cell growth, migration, and differentiation (Belvedere et al., 2020a,b; Olczyk et al., 2015). HS is synthesized as a linear polymer subsequently modified to form mature products with sulfated domains of variable length and composition and responsible of protein ligands (Esko and Lindahl, 2001). HS chains take part of membrane receptors defined HS-proteoglycans (HSPGs) that can modulate the distribution and signaling activity of GFs also acting as co-receptor, as for FGF and its receptor. Therefore, HSPGs act as a GFs reservoir for target cells, by preventing their passive diffusion over longer distances (Matsuo and Kimura-Yoshida, 2014).

* Corresponding author.
** Corresponding author.
E-mail addresses: rbelvedere@unisa.it (R. Belvedere), apetrella@unisa.it (A. Petrella).

https://doi.org/10.1016/j.ejphar.2023.176138
Received 18 July 2023; Received in revised form 2 October 2023; Accepted 18 October 2023
Available online 2 November 2023

The enzymatic cleavage of HSPGs by heparinases induces their release from cell membrane, facilitating GFs movement through the extracellular space. Nevertheless, the precise mechanisms by which HSPGs regulate the distribution and signaling activity of GFs are not fully understood (Yan and Lin, 2009). Heparinases (Hep; endo-β-glucuronidases) selectively cleave heparin and HS chains, producing oligosaccharide products. Three isoforms of bacterial enzyme heparinase have been found differing for the specific site of cleavage on heparin and HS: the heparinase III cleaves undersulfated regions acting predominantly on HS (Boyce and Walsh, 2022). Heparinase III retains an HS-degrading activity highly equivalent to the heparanase, the mammalian enzyme, releasing more bioactive HS chains than the native counterparts (Jones et al., 2004; Dong et al., 2012; Patel et al., 2007).

In human, relatively high heparanase expression levels have been noted in skin tissue, possibly correlating with keratinocyte differentiation. After skin injury, high levels of Hep have been recorded by migrating keratinocytes and in the granulation tissue suggesting that this enzyme may play a role in the course of wound healing (Zcharia et al., 2005). Nevertheless, in this last process low evidences have been highlighted about the role of Hep. However, the degradation of HS results in releasing GFs bound to the ECM, inducing new blood vessels formation (Nasser, 2008).

In the wealthy scenario of commercially available biomaterials for wound healing the investigation about advanced pharmacological therapies is still necessary (Freedman et al., 2023). Novel mechanisms represent the objective of advanced studies aimed to the active vascularization and cell recruitment. Here, we tested for the first time the activity of the triple association, intended as co-administration, among GFs (as EGF, FGF and VEGF), HS and Hep in *in vitro* and *in vivo* models of wound healing. Our outcomes allowed us to consider this mixture an attractive potential treatment for skin wounds and a subject worthy of future in-depth studies.

2. Materials and methods

2.1. Cell cultures and treatments preparation

HaCaT cell line (Human immortalized keratinocytes; CLS, Cell Lines Service GmbH, Eppelheim Germany) and BJ cell line (Human immortalized fibroblasts; American Type Culture Collection, ATCC, Manassas, VA USA) were cultured as reported in (Belvedere et al., 2018a,b). HUVEC cell line (Human umbilical vein endothelial cells; ATCC, Manassas, VA USA) was maintained until passage 10 as reported in (Belvedere et al., 2017).

HS (Laboratori Derivati Organici -LDO- S.p.a.; Trino, VC, Italy) was dissolved in phosphate buffered solution (PBS) and used at the final concentration of 10 μg/ml (Belvedere et al., 2020a,b). EGF (Recombinant Human EGF; Gibco; Waltham, MA, USA), bFGF (Recombinant Human FGF-b; Gibco; Waltham, MA, USA) and VEGF (Recombinant Human VEGF 165 Protein; R&D Systems; Minneapolis, MN, USA) were dissolved in PBS reaching a final concentration of 10 ng/ml as indicated in (Belvedere et al., 2017). Heparinase III (Hep, Sigma-Aldrich; Saint Louis, MO, USA) was prepared in a buffer based on 20 mM TRIS-HCl pH 7.5, 0.1 mg/ml bovine serum albumin (BSA) and 4 mM $CaCl_2$ in deionized water and was used at the final concentration of 6 units (U) (1U of enzyme has been considered able to convert 0.1 μmol of HS).

2.2. (3-(4,5-dimethylthiazol-2-yl)-2,5-diphenyltetrazolium bromide) MTT assay

MTT assay was conducted seeding cells at 8×10^3 cells/well in a 96-well plate and incubated for the indicated times at 37 °C. At the ends of the selected experimental times, MTT stock solution (5 mg/ml) was added to all wells of an assay (25 μl per 100 μl medium), and plates were incubated at 37 °C for 4 h. At the end of each experimental point, cells were lysed by using 100 μl of DMSO. The optical density (OD) of each well was measured with a microplate spectrophotometer (Titertek Multiskan MCC/340) equipped with a 550 nm filter. The viability of cells in response to treatment with tested compounds was calculated as: % viable cells = [OD treated cells/OD negative control] × 100.

2.3. In vitro wound-healing and invasion assays

In a 12-well plastic plate, HaCaT, BJ and HUVEC cells were seeded (density of 2×10^5 and 1×10^5, and 2×10^5 cells, respectively, per well). After 24 h at 100% confluency a wound was made in the cellular monolayer by gently scraping the cells with a sterile plastic p10 pipette tip. All experimental points were further treated with mitomycin C (10 μg/ml, Sigma-Aldrich; Saint Louis, MO, USA) to ensure the block of mitosis. The assay and the following analysis were performed as reported in (Belvedere et al., 2020b, 2021). Briefly, the wounded cells were incubated at 37 °C in a humidified and equilibrated (5% v/v CO_2) incubation chamber of an Integrated Live Cell Workstation Leica AF-6000 LX (Leica Microsystems CMS Gmbh, Wetzlar, Germany). A 10× phase contrast objective was used to record cell movements with a frequency of acquisition of 10 min on at least 10 different positions for each experimental condition. The migration rate was determined for at least 10 different cells randomly selected on each wound edge by measuring the distances covered from the initial time to the selected time-points. The Leica ASF software (bar of distance tool, Leica ASF software, version Lite 2.3.5, Leica Microsystems CMS Gmbh, Wetzlar, Germany) was used.

Cell invasiveness was studied using the trans-well cell culture (12 mm diameter, 8.0 pore size; Corning Incorporated, New York, NJ, USA), as previously described (Belvedere et al., 2014). Briefly, the chambers, coated with matrigel (Becton Dickinson Labware; Franklin Lakes, NJ, USA) in a dilution 1:3 of serum-free medium, were stored at 37 °C until its gelation. Cells were plated in 350 μl of serum-free medium (5×10^4/insert) in the upper chamber of the trans-well. In the lower chamber a volume of 1.4 ml of growth medium was put with the treatments. Then the trans-wells were left for 24 h at 37 °C in 5% CO_2-95% air humidified atmosphere. After that, the medium was aspirated, the filters were washed twice with PBS 1 × and fixed with p-formaldehyde (4% v/v in PBS; Lonza, Basel, Switzerland) for 10 min, then with 100% methanol (Sigma-Aldrich; Saint Louis, MO, USA) for 20 min. The filters so fixed were stained with 0.5% crystal violet prepared from stock crystal violet (powder, Merck Chemicals; Darmstadt, Germany) by distilled water and 20% methanol (Sigma-Aldrich; Saint Louis, MO, USA) for 15 min. Then, the filters were washed again in PBS 1 × and cleaned with a cotton bud. The cells migrated to the lower surface were counted in twelve random fields using EVOS optical microscope (10×) (Life technologies Corporation; Carlsbad, CA, USA).

2.4. Haemocytometer counting

In order to measure cell proliferation, we performed the haemocytometer counting. In detail, HaCaT, BJ and HUVEC cells were seeded in a 12- well-plate (1×10^4 cells/well). After 12 h of serum starvation to obtained cell cycle synchronization, cells were harvested at 24, 48, and 72 h from treatments (Belvedere et al., 2020b). The cell counting was performed as reported in (Bizzarro et al., 2019). In particular, equal volumes of 0.4% trypan blue staining solution (Sigma-Aldrich, St. Louis, MO, USA) and of the cell suspension were mixed. Approximately 10 μl of trypan blue/cell mix was put at the edge of the coverslip of the Burker chamber and the haemocytometer grid was visualized under the optical microscope Axiovert 40 CFL (Carl Zeiss Microscopy GmbH, Jena, Germany). To calculate the viable cells/ml, the average number of cells in one large square was multiplied by the dilution factor (2) and then by 10^4.

2.5. Tube formation assay

As reported in (Belvedere et al., 2021a,b), HUVEC cells were added to the top of the gelated matrigel at a density of (2×10^4 cells/well) in the presence or absence of the treatments indicated for each experimental point. After 12 h, the images were captured using the EVOS optical microscope (10 ×) (Life technologies Corporation, Carlsbad, CA, USA) (Belvedere et al., 2020b). Subsequent analyses both for length of each tube and the number of branches, were carried out using the ImageJ software (NIH, Bethesda, MD, USA; Angiogenesis Analyzer for ImageJ).

2.6. Confocal microscopy

HaCaT, BJ and HUVEC cells were fixed in p-formaldehyde (4% v/v in PBS; Lonza, Basel, Switzerland). Once permeabilized with Triton X-100 (0.4% v/v in PBS; Lonza, Basel, Switzerland), they were blocked with goat serum (20% v/v in PBS; Lonza, Basel, Switzerland) as reported in (Belvedere et al., 2016, 2021). Next, the cells were incubated with mouse monoclonal anti-fibronectin (1:100; Abcam, Cambrige, UK), anti-vimentin (1:250; Santa Cruz Biotechnologies, Dallas, TX, USA), anti-vinculin (1:100; Santa Cruz Biotechnologies, Dallas, TX, USA), and anti-E-cadherin (1:500, BD Transduction Laboratories, San Jose, CA), overnight (O/N) at 4 °C. F-actin was evaluated by 5 μg/ml of Phalloidin-FITC (Sigma-Aldrich; Saint Louis, MO, USA) for 30 min, at room temperature (RT) in the dark. The staining with conjugated anti-mouse antibodies and the nuclei and the confocal evaluation with was performed as described in (Bizzarro et al., 2017).

Confocal microscopy analysis was also performed in mouse skin biopsies. The cryosections were fixed in 4% paraformaldehyde, washed in PBS, permeabilized in 0.5% Triton X-100 (5 min) and, finally, blocked in a blocking buffer containing 20% FBS and 0.05% Triton X-100 (30 min). The sections were then incubated O/N in blocking buffer with mouse primary antibodies against vimentin (1:100, Santa Cruz Biotechnologies, Dallas, TX, USA), FAP1α (1:100; Santa Cruz Biotechnologies, Dallas, TX, USA), CK10 (1:100, Santa Cruz Biotechnologies, Dallas, TX, USA), and with primary rabbit antibody against CD31 (1:100; Abcam, Cambrige, UK). The staining with conjugated secondary antibodies and the nuclei, the confocal analysis (objective 40×) and the quantification from multichannel images obtained were performed as previously described (Belvedere et al., 2018b). Quantifications were performed from multichannel images obtained using a 40× objective using ImageJ (NIH, Bethesda, MD, USA). It was marked either the cell perimeter or the nucleus as the region of interest and calculating integrated densities per area from the appropriate channel. A minimum of 50 cells were analysed for each data set. The obtained mean value was used to compare experimental groups.

2.7. In vivo wound model

C57BL/6 female mice of 6–8 week-old were obtained from (Charles River Italia srl; Milan, Italy) and bred under pathogen-free conditions in the Animal Facility of the University of Salerno. Animal experiments were approved by the Italian Health Ministry (authorization n. 489/2018-PR) and performed according to Italian law 26/2014. Mice were anesthetized by inhalation of isoflurane, shaved, and cleaned. The adequacy of anesthesia during the whole procedure was confirmed by monitoring the respiratory rate and depth and by the absence of the lower extremity reflex to pressure stimuli. In general, the anesthetic depth was checked regularly for the duration of the procedure. The entire operation was done in a hood, with sterile technique maintained throughout. All the procedure of wound creation and splinting is reported in (Belvedere et al., 2021a,b; Wang et al., 2013). Briefly, full-thickness wounds were made in the doughnut region of the splint using 6-mm-diameter punches (Acuderm, Fort Lauderdale, FL, USA). The wounds were produced by the surgical removal of all skin layers (epidermis, dermis and subcutaneous fat) from the animal. Around the wounds a sterile silicone sheet ring was carefully placed previously treated with an instant-bonding adhesive (super attak, Loctite®; Henkel, Milan, Italy) to reduce the contraction of the wounds. Each wound was centred within this created splint. All treatments were applied dissolving in PBS which was also used as control on one wound of each mouse. The treatments were performed on the wound of the right side, while the control wounds, that were the PBS experimental points, were on the left side of the same mouse. Mice were treated at 48 h of time intervals from 0 to 10 days, photography reportage was obtained at 0 and 10 days. The percentage of the initial wound that remained open was quantified as difference between 0 and 10 days. Thus, the final wound region, at day 10, was measured compared to the same one at day 0 and the differently treated area was compared to the related control one on the same back. After the mice were sacrificed, the skin wounds were harvested at about 50 mm on the side of lesions including both of them for each sample biopsy. They were washed and fixed in a solution of p-formaldehyde (4% v/v in PBS; Lonza, Basel, Switzerland). Then, biopsies were incubated in a sucrose solution to guarantee the cryoprotection. The frozen sections were cut on a Leica CM 1950 cryostat (Leica Microsystems CMS Gmbh, Wetzlar, Germany) at 5 μm, mounted directly on super frost slides (Thermo Fisher Scientific Inc. Waltham, MA, USA) for H&E staining performed as reported in (Novizio et al., 2021) and microscopy analysis.

2.8. Western blotting

Protein expression was examined by SDS-PAGE, as described in (Festa et al., 2009). Total intracellular protein content, obtained by RIPA lysis buffer (containing protease inhibitors), was estimated according to Biorad protein assay (BIO-RAD; Hercules, CA, USA). A total of 20 μg of proteins were analysed using the chemiluminescence detection system (Amersham biosciences; Little Chalfont, UK) after incubation with primary antibodies against ERK (rabbit monoclonal; 1:1000; Cell Signaling Technology, Danvers, MA, USA), p-ERK (rabbit monoclonal; 1:1000; (Thr202/Tyr204); Cell Signaling Technology, Danvers, MA, USA), FAK (rabbit monoclonal; 1:1000; Cell Signaling Technology, Danvers, MA, USA), p-FAK (rabbit monoclonal; 1:1000; Cell Signaling Technology, Danvers, MA, USA) and Glyceraldehyde-3-Phosphate DeHydrogenase (GAPDH; mouse monoclonal; 1:1000; Sigma-Aldrich, Saint Louis, MO, USA) O/N at 4 °C and the related secondary anti-mouse/rabbit antibodies. The blots were exposed to Las4000 (GE Healthcare Life Sciences, Little Chalfont, UK) and the relative band intensities were determined using ImageQuant software (GE Healthcare Life Sciences, Little Chalfont, UK).

2.9. Statistical analysis

As reported in (Belvedere et al., 2017), statistical analyses were carried out using Microsoft Excel (Redmond, WA, USA). The number of independent experiments, standard deviation, and p-values are indicated in the figure legends. All results are the mean ± standard deviation (SD) of at least 3 experiments performed in triplicate. Statistical comparisons between groups were made using two-way ANOVA or unpaired, two-tailed *t*-test comparing two variables. $p < 0.05$ indicated significant differences.

3. Results

3.1. The association of HS + Hep + EGF promotes keratinocytes and fibroblasts migration and invasion

We have first tested the migration and invasion abilities of human keratinocytes and fibroblasts in presence of HS, EGF/FGF and Hep, and all their combination, including the whole association (HS + EGF/FGF + Hep). We choose to use the heparinase III isoform which has been reported to be selective for HS (Chappell et al., 2008; Hoogewerf et al.,

1995). Moreover, the amount of HS has been selected as 10 μg/ml, following a concentration/response curve (from 100 ng/ml to 100 μg/ml) on all the three cell lines here utilized to evaluate first their viability and then the motility. Thus, we have confirmed, as shown in other *in vitro* models (Belvedere et al., 2020a,b), that in no case HS has affected cell health and that, starting from 10 μg/ml, it has promoted the more interesting migration speed (see Supplementary Fig. S1). In relation to this, 6U of Hep have been used.

As shown in Fig. 1A and B, the treatment of HaCaT cells with HS and EGF separately induced an important acceleration for both processes. Interestingly, when we have administered together the two molecules (HS + EGF), we have assisted to a notable slowdown of cell migration/invasion. In this case, even still statistically significant, the levels of cell rate returned similar to control. When the association between HS and EGF was further combined with Hep, meaning the whole combination HS + EGF + Hep, the induction of migration and invasion speed acquired a more significant pulse. Treatment of cells with Hep alone did not influence both processes. In Fig. 1C, we reported the count of HaCaT cells, assessing that in presence of the EGF alone and in co-treatment with Hep, the proliferation was significantly induced, at 24, 48 and 72 h. HS retained no effects on this process, neither alone nor associated to Hep. Surprisingly, if associated to HS and Hep, EGF showed a greater effect in the promotion of keratinocytes growth. This pronounced activity became more evident at 48 and 72 h of treatment.

Similarly to what we have found on keratinocytes, the BJ cells showed a very comparable tendency in presence of the same kind of treatments (considering that in this case EGF has been substitute by FGF). In particular, both for migration (Fig. 1D) and for invasion processes (Fig. 1E), the mixture of FGF and HS together with Hep (HS + FGF + Hep) was able to promote a notable induction of fibroblast motility. This result reached a more interesting assessment if compared to the administration of HS or FGF alone, with or without Hep. Indeed, the treatments HS and HS + Hep, FGF and FGF + Hep retained a very similar tendency among them, more pronounced than control but significantly less than the whole mixed. Moreover, as for HaCaT cells, FGF + HS treatment showed a slower behaviour in the evaluation of both migration and invasion. In no case Hep, when added alone, induced a change on the analysed processes. Finally, in Fig. 1F BJ cells, analysed through haemocytometer counting, showed a marked proliferation rate in presence of FGF and FGF/Hep at 24, 48 and 72 h. In parallel with HaCaT cells, HS had no effects and the mix of the three elements showed a greater effect in the promotion of cells growth above all at 48 and 72 h.

3.2. The combination HS + Hep + VEGF favours the motility of endothelial cells and the in vitro angiogenesis

The importance of angiogenesis in wound healing led us to the investigation of the response of HUVEC cells to HS and VEGF in presence or not of Hep. In Fig. 2A, we showed the induction of a significant migration speed of endothelial cells in presence of the whole combination composed by HS + VEGF + Hep. This assessment was the most markable with respect to the other ones. Indeed, as for keratinocytes and fibroblasts, HS, with and without Hep, and the GF, in this case VEGF, with and without Hep, promoted cell migration. On the other hand, a similar stimulus was not recorded on HUVEC treated with HS + VEGF revealing an outcome comparable to not treated cells. The same tendency was found in case of invasion process (Fig. 2B). Finally, we assessed the *in vitro* angiogenesis as reported in Material and method section. Particularly, the analysis of the number of branching points and the tubes length in Fig. 2D and E revealed that HS or VEGF acted as promoters of the process, both alone and with the enzyme. Also when administered together as HS + VEFG, they induced a pro-angiogenic stimulus similar to the other experimental points. Finally, the ability of HUVEC cells to structure themselves in capillaries acquired the best condition in case of the addition of all the elements associated (HS + VEGF + Hep) (Fig. 2D and E and C for the representative images).

Fig. 2F reports the count of HUVEC cells. In presence of VEGF, endothelial cells proliferation was significantly induced at 24, 48 and 72 h compared to control, to Hep and HS. Moreover, if associated to HS and Hep, the growth factor showed a bigger effect in the promotion of HUVEC proliferation at 48 and 72 h.

3.3. Keratinocytes activation is induced by the association HS + Hep + EGF

To migrate over the wound site, keratinocytes must reorganize their cytoskeleton increasing the contractility forces, mainly focusing on F-actin polymerization, which is essential for motility (Yan et al., 2016). Therefore, we analysed the HaCaT F-actin organization by phalloidin staining highlighting a slight and cortical signal in not-treated and Hep-treated cells (Fig. 3A, panels a and d). On the contrary, stress fibers appeared after 24 h from the administration of HS and HS + Hep and EGF and EGF + Hep (Fig. 3A, panels c, f, b and g). Additionally, while presenting a strong signal, F-actin did not show a structure supporting migration in presence of HS + EGF (Fig. 3A, panel e). This situation completely changed when we added the enzyme to this last association (HS + EGF + Hep). In this case, protein polymerization in stress fibers became evident with the generation of the tensile forces to facilitate HaCaT motility (Fig. 3A, panel h). Furthermore, epithelial cell polarization receives an important stimulus by E-cadherin activity: this protein controls the switch from adhesive to migratory keratinocyte phenotype (Halbleib and Nelson, 2006). For this reason, we investigated its expression and localization in HaCaT cells finding that, mainly in presence of HS with and without Hep, cells strongly lost the signal (Fig. 3B, panels k and n). This tendency appeared less dependent on EGF, if alone or accompanied by Hep or HS (Fig. 3B, panels j, m, o). Finally, E-cadherin almost completely disappeared when the whole association was administered to keratinocytes (Fig. 3B, panel p).

The co-administration of HS, Hep and EGF promoted higher expression levels of the Focal Adhesion Kinase (FAK) protein and of its tyrosine-phosphorylated form (p-FAK) (Fig. 3C), a well-known protein involved in some mechanotransduction pathways in wound repair (Januszyk et al., 2017; Pessolano et al., 2021). An intermediate condition was obtained following treatments based on HS and EGF. In detail, the basal low expression of FAK, and consequently p-FAK underwent a marked increase in a HS-mediated manner above all when this molecule was differently combined to reach the maximum level in presence of the whole mixture (Fig. 3D). Furthermore, according to the different degree of cell proliferation previously highlighted through haemocytometer counting, we also assessed the phosphorylated, as active, form of the Extracellular signal-Regulated Kinase (ERK). We observed that the major degree of activation was induced by the complete combination of our interest (Fig. 3C and D). Also in this case, only a middle signal was evaluated in presence of HS, HS + Hep and HS + EGF (Fig. 3C and D). A slightly higher expression was found dependent of EGF, meaning the greater effect of the growth factor on the activation of ERK-triggered pathway. As expected, the total form of ERK did not undergo any change in term the expression.

3.4. Fibroblasts switch is triggered by HS and FGF and it is enhanced in presence of Hep

In an analogous manner, we investigated the organization of F-actin cytoskeleton in BJ cells. In fibroblasts these filaments strongly organized to generate force driving movement (Belvedere et al., 2018a,b) in case of all treatments based on HS and FGF alone and particularly with Hep but not HS + FGF (Fig. 4A, panels b, c, e, f, g). Indeed, only when both molecules were associated to the enzyme the highest degree of F-actin organization has been reached (Fig. 4A, panel h). Moreover, in order to confirm the increment of traction stress forces, our confocal analysis also proved the increase of the expression of vinculin (Novizio et al., 2020). In Fig. 5B, panels i–p, white arrows indicated the presence of this protein

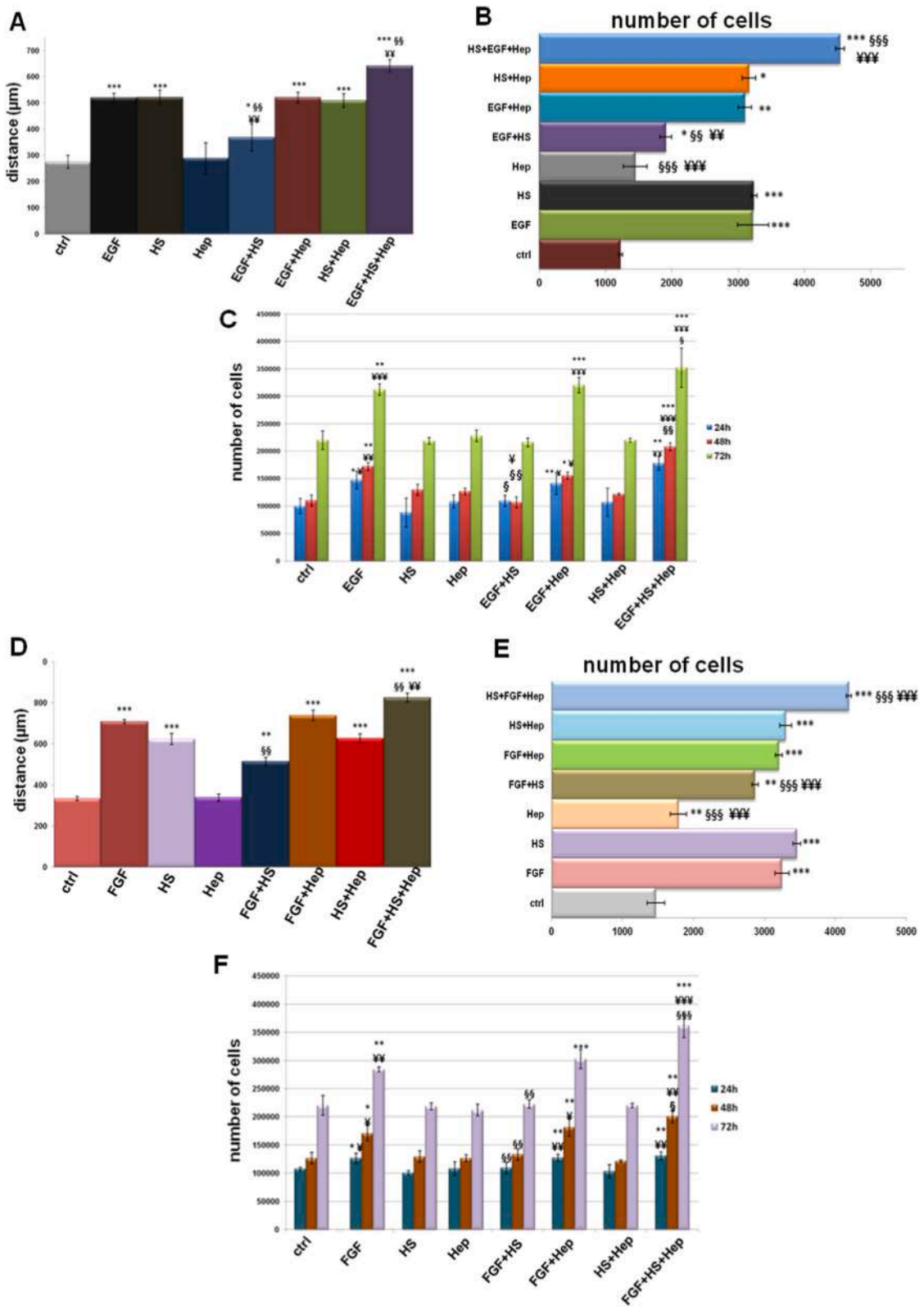

Fig. 1. Analysis of migration and invasion of HaCaT and BJ cells. (**A**) Results from the migration assay on HaCaT treated or not for 24 h with HS 10 µg/ml, Hep 6U, EGF 10 ng/ml alone or differently mixed together. (**B**) Results of the invasion of HaCaT at the same experimental points. (**C**) HaCaT count at 24, 48 and 72 h of treatments. (**D**) Wound healing assay on BJ cells treated or not for 24 h with HS 10 µg/ml, Hep 6U, FGF 10 ng/ml alone or differently mixed together. (**E**) Invasion of BJ at the same experimental points. (**F**) BJ count at 24, 48 and 72 h of treatments. Statistical comparisons between groups were made using two-way ANOVA or unpaired, two-tailed *t*-test comparing two variables, *p < 0.05, **p < 0.01, ***p < 0.001 versus controls; §p < 0.05, §§p < 0.01, §§§p < 0.001 versus HS treated cells; ¥p < 0.05, ¥¥p < 0.01, ¥¥¥p < 0.001 versus EGF treated cells. The data are representative of n = 3 independent experiments ± SD, for the invasion assay data represent the mean of cell counts of 15 separate fields per well.

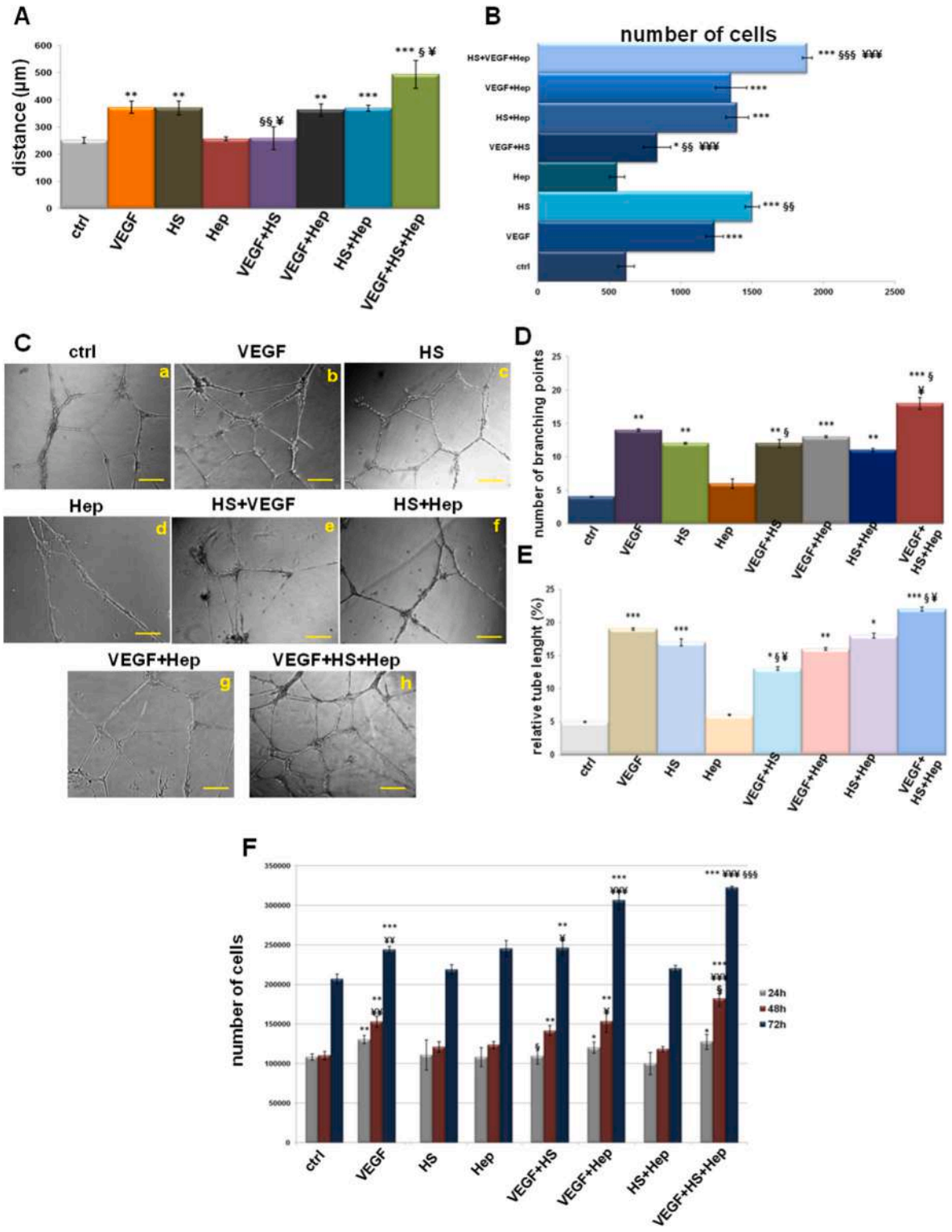

Fig. 2. Assessment of migration and invasion and angiogenesis of HUVEC cells. (**A**) Results from the migration assay on HUVEC treated or not for 24 h with HS 10 μg/ml, Hep 6U, VEGF 10 ng/ml alone or differently mixed together. (**B**) Results of the invasion of HUVEC at the same experimental points. (**C**) Representative images of tube formation. Bar = 100 μm. (**D**) and (**E**) Analysis of number of branches and the tube length, respectively, calculated by ImageJ (Angiogenesis Analyzer tool) software on HUVEC cells equally treated. (**F**) HUVEC count at 24, 48 and 72 h of the described treatments. The data represent a mean of n = 3 independent experiments ± SD. Statistical comparisons between groups were made using two-way ANOVA or unpaired, two-tailed *t*-test comparing two variables, *p < 0.05, **p < 0.01, ***p < 0.001 versus untreated control; §p < 0.05, §§p < 0.01, §§§p < 0.001 versus HS treated cells; ¥ p < 0.05, ¥¥p < 0.01, ¥¥¥p < 0.001 versus VEGF treated cells.

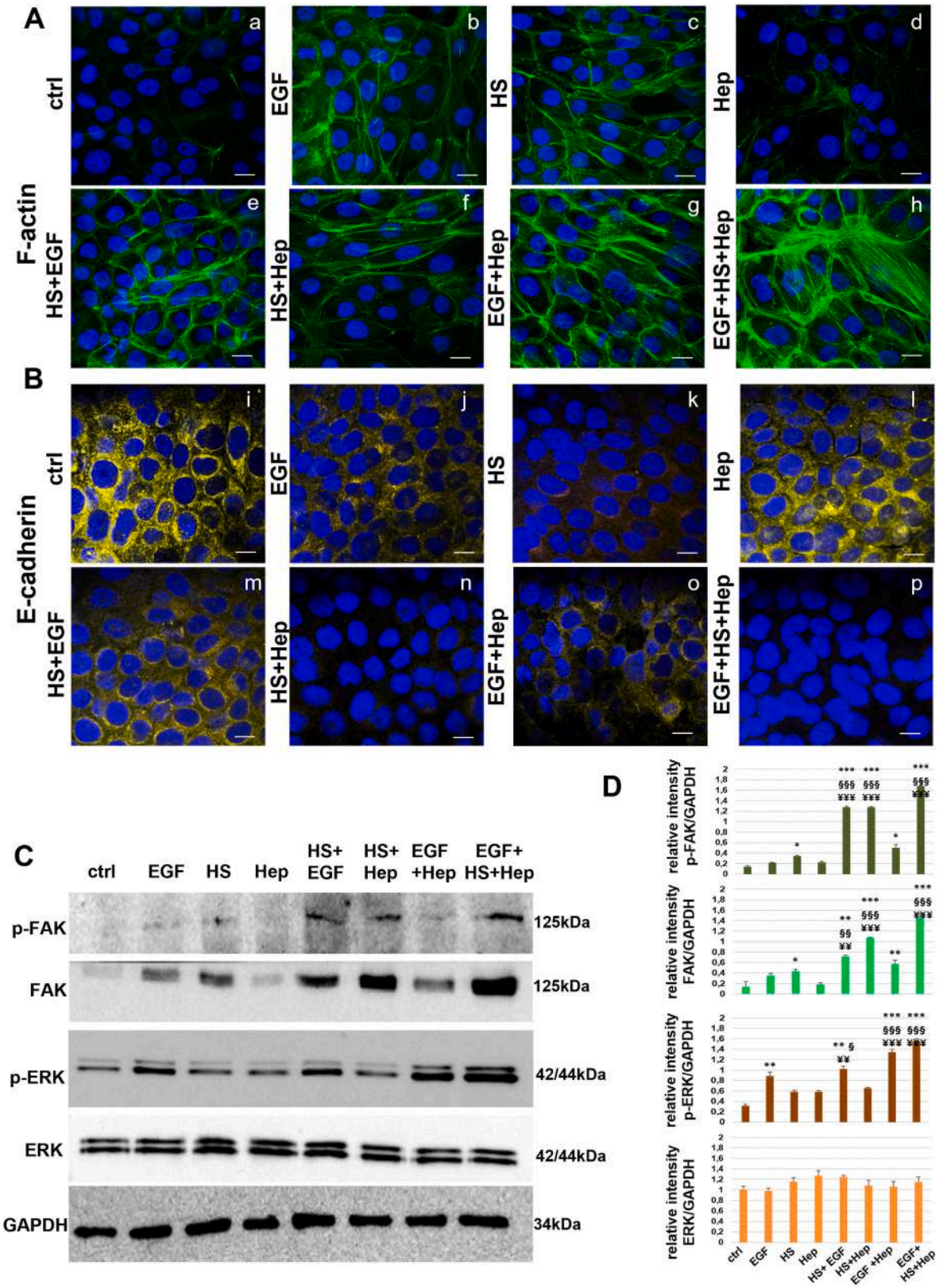

Fig. 3. Analysis of the acquisition of a pro-migratory phenotype of keratinocytes. Immunofluorescence evaluation of (**A**) F-actin (panels a–h) and (**B**) E-cadherin (panels i–p) after treatments with HS 10 μg/ml, Hep 6U and EGF 10 ng/ml alone and differently combined together for 24 h. Bar = 100 μm. (**C**) Western blotting for FAK, phosho-FAK and ERK, phospho-ERK on HaCaT cells at the same experimental points after 24 h and 15 min from treatments, respectively. Protein normalization was performed on GAPDH levels and the relative intensities of signals have been reported in (**D**). The data represent a mean of n = 3 independent experiments ± SD *p < 0.05, **p < 0.01, ***p < 0.001 versus untreated control; §p < 0.05, §§p < 0.01, §§§p < 0.001 versus HS treated cells; ¥¥p < 0.01, ¥¥¥p < 0.001 versus VEGF treated cells.

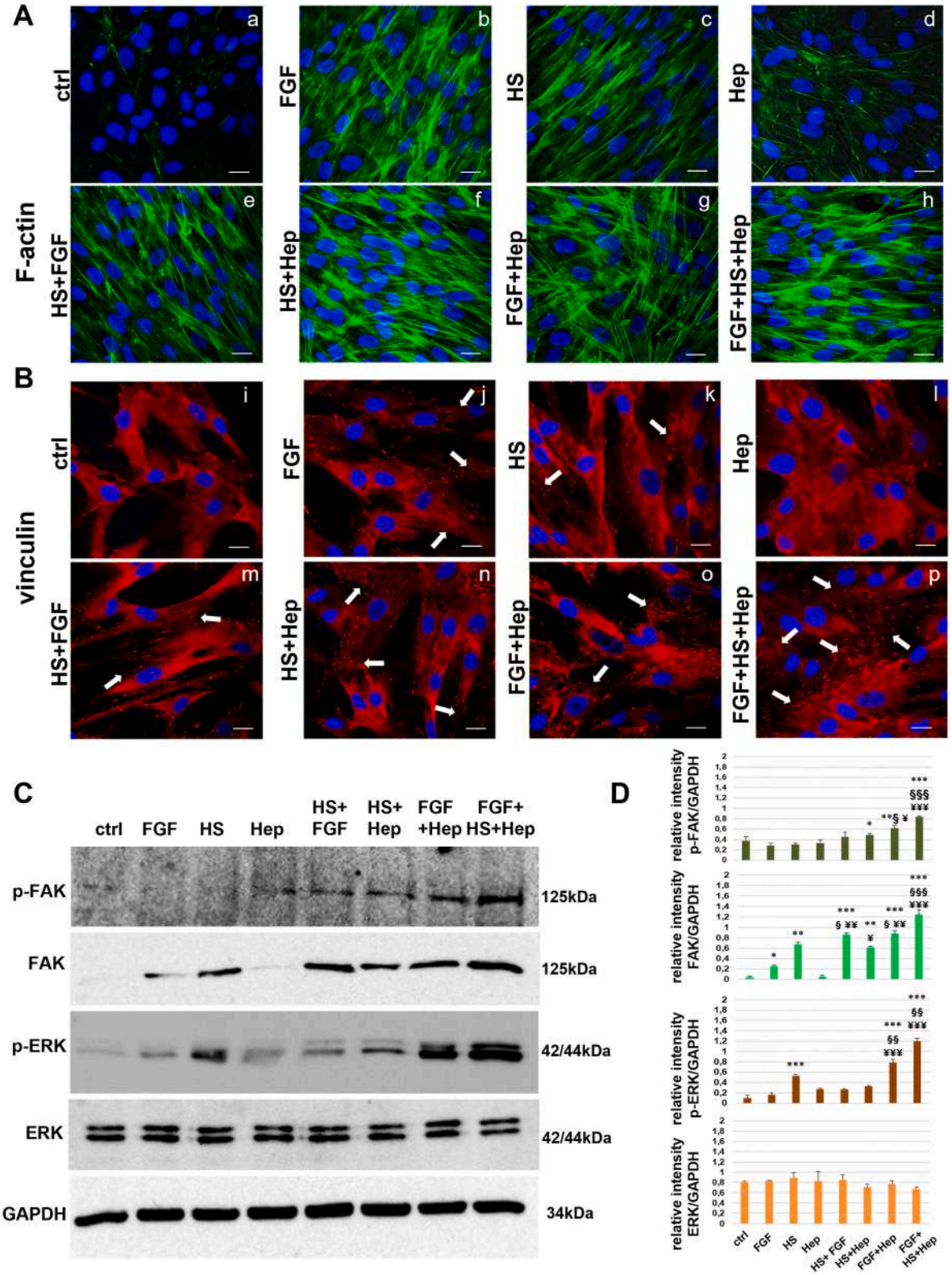

Fig. 4. Evaluation of fibroblasts differentiation. Immunofluorescence analysis on fibroblasts to detect (**A**) F-actin (panels a–h) and (**B**) vinculin (panels i–p) after treatments with HS 10 μg/ml, Hep 6U and FGF 10 ng/ml alone and differently combined together for 24 h. Bar = 100 μm. The major expression of vinculin is indicated with white arrows. (**C**) Western blotting using antibodies against FAK, phosho-FAK and ERK, phospho-ERK on protein content of BJ cells, after 24 h and 15 min from treatments, respectively. Protein normalization was performed on GAPDH levels and the relative intensities of signals have been reported in (**D**). *p < 0.05, **p < 0.01; ***p < 0.001 versus untreated control; §p < 0.05, §§p < 0.01, §§§p < 0.001 versus HS treated cells; ¥ p < 0.05, ¥¥p < 0.01, ¥¥¥p < 0.001 versus VEGF treated cells. The data represent a mean of n = 3 independent experiments ± SD.

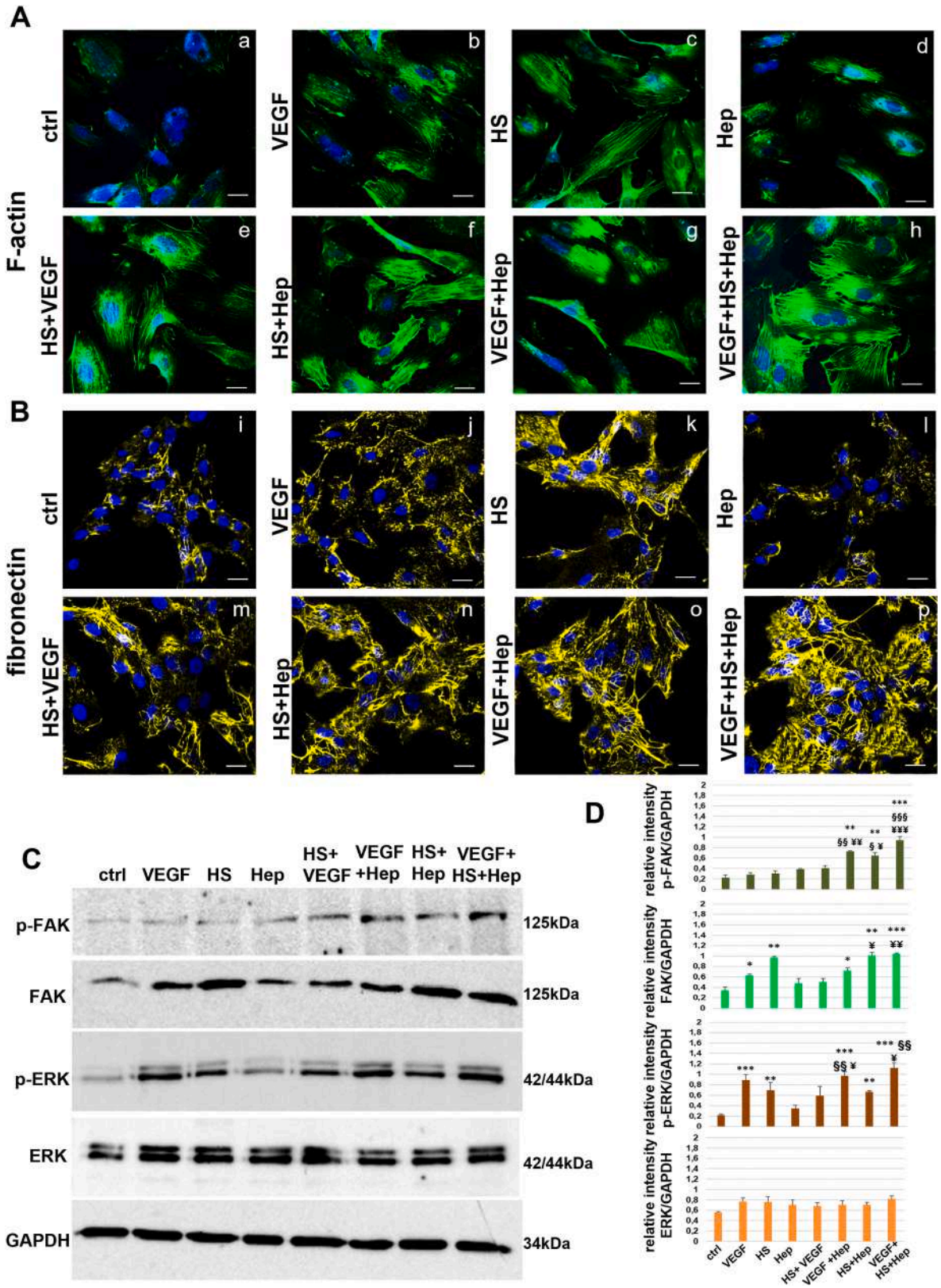

Fig. 5. Examination of endothelial cells activation. Immunofluorescence analysis on HUVEC for (**A**) F-actin (panels a–h), (**B**) fibronectin (panels i–p) after treatments with HS 10 μg/ml, Hep 6U and VEGF 10 ng/ml alone and differently associated together for 24 h. Bar = 100 μm. (**C**) Western blotting using antibodies against FAK, phosho-FAK and ERK, phospho-ERK on protein content of endothelial cells, after 24 h and 15 min from treatment, respectively. Protein normalization was performed on GAPDH levels and the relative intensities of signals have been reported in (**D**). *p < 0.05, **p < 0.01, ***p < 0.001 versus untreated control; §p < 0.05, §§p < 0.01, §§§p < 0.001 versus HS treated cells; ¥p < 0.05, ¥¥p < 0.01, ¥¥¥p < 0.001 versus VEGF treated cells. The data represent a mean of n = 3 independent experiments ± SD.

at the leading edges of fibroblasts which, in this way, showed themselves ready to move when treated with HS and/or FGF (Fig. 4B, panels j, k, m, n, o). As for the other protein markers analysed also on keratinocytes, the major number of vinculin spotted signals was seen in fibroblasts treated with all the three elements (Fig. 4A, panel p).

Fig. 4C and D confirmed that also in BJ cells, the whole mixture of HS + FGF + Hep was able to promote the increase of protein indicated, FAK and its phosphorylated counterpart p-FAK and p-ERK. Also in this case, ERK as total protein form, remained unaffected.

3.5. When mixed to Hep, HS and VEGF association promote endothelial cells activation

In response to tissue injury, endothelial cells acquire a migratory phenotype invading the vascular basement membrane and express mesenchymal markers (Dejana et al., 2017). In this scenario, we first studied F-actin whose organization appeared correspondent to the significant ability of HUVEC cells to differentially migrate in presence of HS, VEGF and Hep opportunely mixed together (Fig. 5A). Indeed, protein polymerization following HS and VEGF alone and together with Hep but less to HS + VEGF (Fig. 5A, panels b, c, e, f, g), reaching the better filamentous structure in presence of all substances (VEGF + HS + Hep) (Fig. 5A, panel h). Furthermore, among the activation protein markers of endothelial cells, we choose to evaluate fibronectin which is known to be able to promote cell migration through cytoskeletal reorganization (Belvedere et al., 2017). Interestingly, the immunofluorescence assay confirmed the greatest fibronectin expression after 24 h of treatments with the whole association (VEGF + HS + Hep) (Fig. 5B, panel p) and an intermediate signal, compared to control and Hep experimental points, in HUVEC cells treated with HS, VEGF, HS + Hep, VEGF + Hep or HS + VEGF (Fig. 5B, panels j, k, m, n, o).

As for HaCaT and BJ, HUVEC cells expressed high levels of FAK protein, both as phosphorylated in its tyrosine 397 residue and not, after treatments with HS alone, and in combination with Hep and with Hep + VEGF (Fig. 5C and D). Finally, while ERK appeared unchanged, the phospho-ERK levels increased following the effects of VEGF more than HS ones (Fig. 5C and D). Also in this case, the action of the growth factor was strongly emphasized when associated to both HS and Hep.

3.6. The association of HS, GFs and Hep stimulates skin wound repair in vivo

We then evaluated the effects of HS, GFs and Hep in an *in vivo* system. We tested the effects of these substances in C57BL/6 mice on which we have created two intrascapular skin wounds. For each mouse, one wound was locally treated with HS 10 μg/ml, or GFs (as mix of the three factors EGF, FGF and VEGF) 10 ng/ml, Hep 6U or their different types of combination, and the other one with PBS as technical control. As reported in (Belvedere et al., 2021a,b), the wounds were produced by the surgical removal of all skin layers (epidermis, dermis and subcutaneous fat) from the animal and for each wound a surrounding silicone rubber ring was attached to reduce the contraction of the wounds (Meier et al., 2013). The wound areas were recorded by photography for 10 days. First, at day 10 of treatment we found that the single treatment with HS or the mixture of GFs induced a relevant reduction of wound regions compared to PBS on the second wound performed (as macroscopically shown in Fig. 6A where the treated wounds are on the right side, while the control wounds are on the left side, and by the analysis of wound sizes in 6B). A very similar situation was obtained when both HS and GFs were used together with Hep. This result was not so evident in case of Hep treatment alone or of HS + GFs. Importantly, the association HS + GFs + Hep induced a faster wound healing response and reduction of the injured area with respect to each other treatment (Fig. 6A and B). Moreover, the hematoxylin/eosin (H&E) staining of mice skin sections revealed a compact matrix in HS and HS + Hep treated wounds (Fig. 6C, panel b and f) compared to a generally unstructured matrix in control wound (Fig. 6C, panel a). Similar tissue architecture was found in lesions treated with GFs and GFs + Hep accompanied, however, by a relevant presence of vessels (Fig. 7C, panel c and g, yellow arrows). A lower presence of vessels and a less compact matrix were observed in lesions treated with HS + GFs (Fig. 6C, panel e, yellow arrows). The use of the combination HS + GFs + Hep induced the formation of a very well-organized matrix with vessels (Fig. 6C, panel h, yellow arrows) compared to each other treatment. This qualitative aspect acquires a more relevant meaning compared to the slightly increasing degrees of speed of the lesions repair in presence of HS + GFs + Hep.

3.7. Cell activation in mice skin lesions is promoted by the association HS + GFs + Hep

We then verified the presence of fibroblasts, keratinocytes, and endothelial cells in the skin biopsies. We used the vimentin staining as distinguishing feature of a resident mesenchymal “repair” fibroblast population (Belvedere et al., 2022; Chen et al., 2016). The biopsies of skin mice treated for 10 days with the HS, GFs, HS + Hep, GFs + Hep (Fig. 7, panels b, c, f, g, respectively) showed high levels of vimentin in the dermis, compared to the skin treated with PBS (control) and with lesions treated with Hep alone (Fig. 7, panels a and d). A weaker signal was found on lesions treated with HS + GFs (Fig. 7, panel e). Moreover, the treatment with the whole combination HS + GFs + Hep induced a much more marked signal for vimentin proving the high recruitment of fibroblasts which migrate and populate the dermis (Fig. 7, panel h). Besides vimentin, we also showed the presence of Fibroblasts Activated Protein 1α (FAP1α), which is classically attributed to activated fibroblasts. Particularly, in mice skin wounds treated with HS, with and without Hep, the expression level of FAP1α (Fig. 7, panels j and n) in the dermal section of biopsies was significant higher compared with the PBS and with Hep alone (Fig. 7, panels i, and l). A quite lower signal was found in presence of the experimental points including GFs (Fig. 7, panels k and o), mainly if these factors were mixed to HS in absence of Hep (Fig. 7, panel m). When treatments were performed with all molecules a higher signal has been highlighted (Fig. 7, panel p).

Next, we used cytokeratin 10 (CK10), as the earliest proteins expressed during keratinocytes differentiation process. The expression levels of CK10 appeared following the treatment of HS and HS + Hep (Fig. 7, panels r and v). An important upregulation of this protein appeared also in case of GFs and GFs + Hep (Fig. 7, panels s and w) compared with control PBS or the enzyme alone (Fig. 7, panels q and t). Furthermore, CK10 signal became stronger in presence of HS + GFs + Hep (Fig. 7, panel x). Finally, in order to verify the presence of endothelial cells in the skin mice biopsies, we used the endothelial specific marker CD31. In presence of HS and HS + Hep (Fig. 7, panels z and d’) and particularly of GFs and GFs + Hep (Fig. 7, panels a’ and e’) a relevant signal appeared evident in the dermis area compared to the PBS and Hep treated ones (Fig. 7, panels y and b’). Also in this case, CD31 signal decreased in presence of HS + GFs (Fig. 7, panel c’), while the use of the whole combination of our interest induced a significant increase of the protein signal (Fig. 7, panel f’).

4. Discussion

In this work we have demonstrated the *in vitro* and *in vivo* efficacy of the association of GFs and HS in presence of the heparinase enzyme in promoting the major biological processes on the most important cell populations involved in tissue regeneration.

It is known that heparinase is able to cleave HS, generally larger than 3000 Da, in shorter oligosaccharides with a glucuronic acid and N-acetylglucosamine disaccharide sequence at the newly formed reducing end and to remove all binding sites from the proteoglycan by cleaving the HS chain from the core protein (Boyce and Walsh, 2022). Numerous studies use the enzyme of bacterial origin on mammalian *in vitro* and *in vivo* systems as it is the most commercially available product and easier

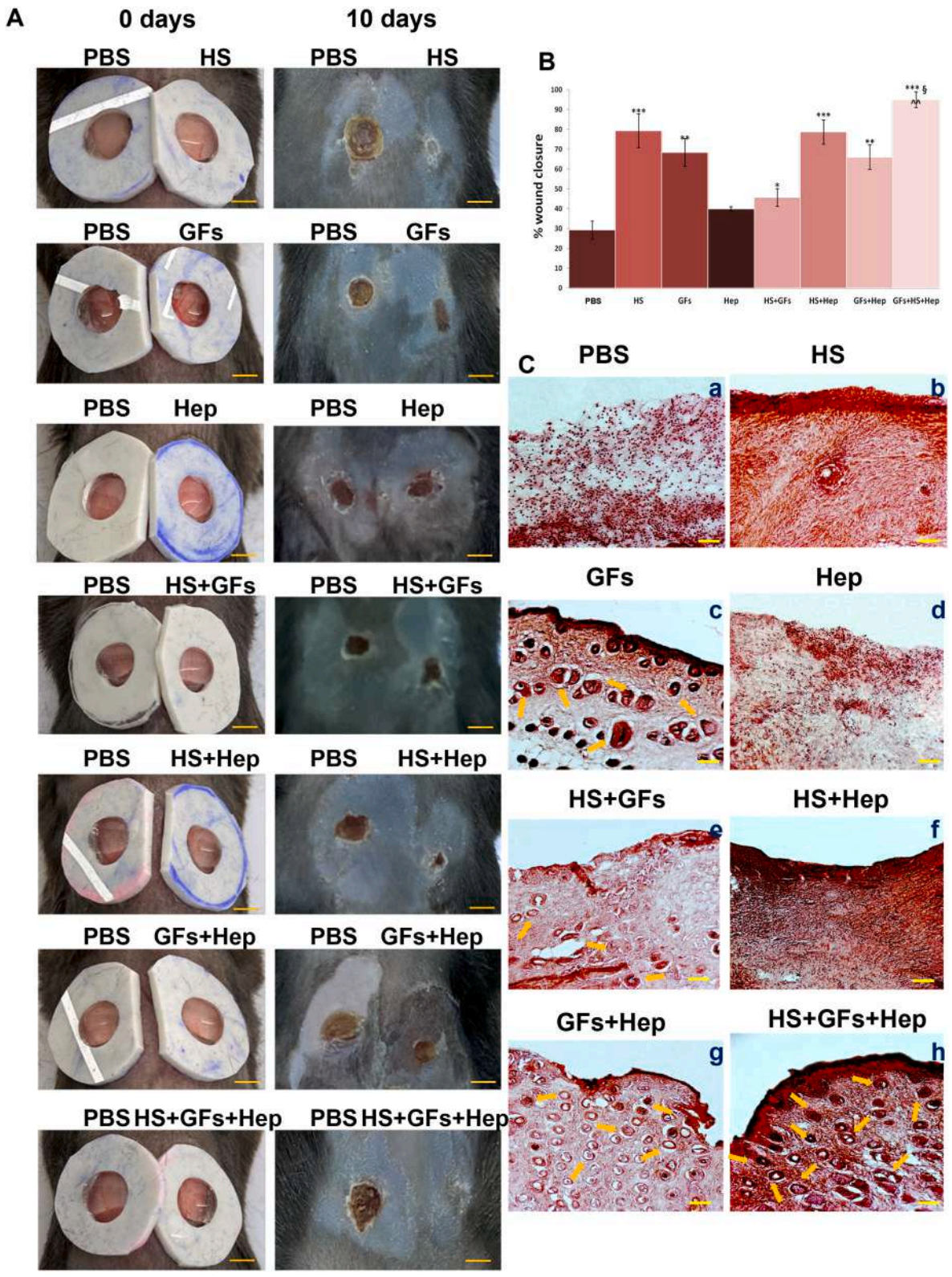

Fig. 6. ***In vivo*** **analysis of skin wound closure.** (**A**) Excisional skin wounds on C57BL6 mice were macroscopically photographed at the indicated time (the day 0 pictures have been taken immediately after injury). Representative results from five individual mice from each group are shown. PBS was administrated on the wounds at the left side while all the other treatments were added on the wounds at the right one. Bar = 5 mm. (**B**) Wound areas measurements at day 10 calculated as percentage as differences with the diameter of the related lesions at day 0. The data represent a mean of n = 3 independent experiments ± SD. Statistical comparisons between groups were made using two-way ANOVA or unpaired, two-tailed *t*-test comparing two variables, *p < 0.05, **p < 0.01, ***p < 0.001 versus PBS treated controls; §p < 0.05 versus HS treated wounds; ^p < 0.01 versus GFs treated lesions. (**C**) Skin sections have been stained through H&E (panels a–h). Vessels are indicated by yellow arrows. Bar = 100 μm.

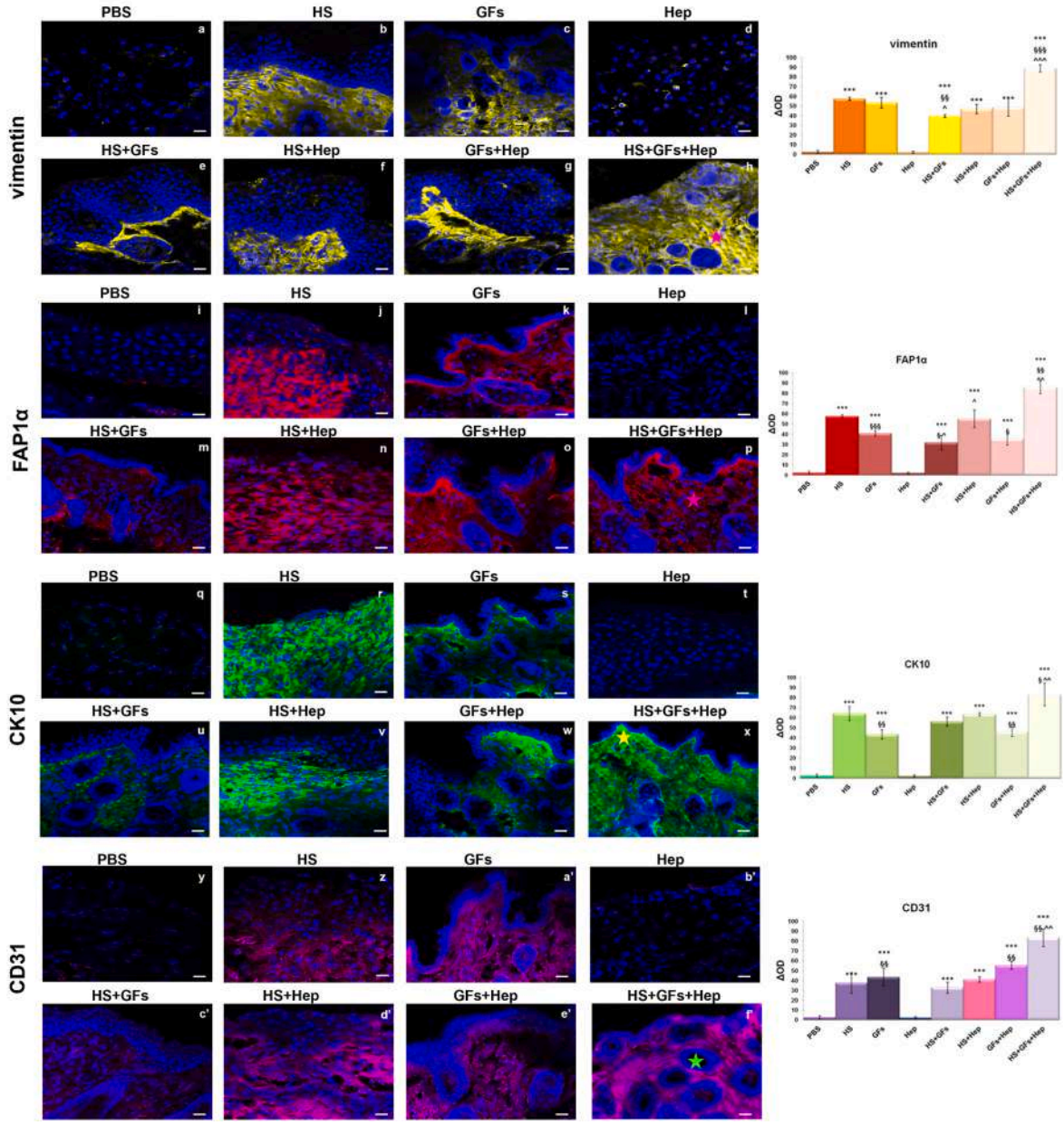

Fig. 7. Immunofluorescence analysis of mice sections. Representative images of vimentin (panels a–h) and FAP1α (panels i–p) (fibroblasts markers, respectively), CK10 (panels q–x) (keratinocytes marker) and finally CD31 (panels y–f') (endothelial cell marker) staining by immunofluorescence in mice wound healing sections. In panels h and p the pink star symbol marks the granulation area; in panel x yellow star marks epidermis; in panel f' the star is a vessel. Nuclei were stained with 4′,6-diamidine-2′-phenylindole dihydrochloride (DAPI) 1:1000 for 30 min at RT in the dark. Densitometry analysis has been performed for each group of images. ***p < 0.001 versus PBS; §p < 0.05, §§p < 0.01, §§§p < 0.001 versus HS; ^p < 0.05, ^^p < 0.01, ^^^p < 0.001 versus GFs.

to purify by standardized technical procedures (Ding et al., 2012; J.W. Park et al., 2017; Zeng et al., 2012; Cerezo-Magaña et al., 2021; Corti et al., 2019). Actually, the HS-degrading efficacy of heparinase and heparanase (hep III and hep-1 isoforms, respectively) has been shown to be highly comparable despite a slight difference in the mechanisms of action (Jones et al., 2004; Dong et al., 2012).

Following heparinase cleavage, also the HS specific binding sites can be destroyed facilitating the transport of the ligands to other sites of action (Bame, 2001). It is therefore plausible that heparinase induces the release of HS-bound GFs (i.e., bFGF, VEGF, EGF) which sustain neovascularization and wound healing (Masola et al., 2018). Hence, it is conceivable that once degraded by heparinase, HS could lose this role of sequestrator to mediate the release of ECM-resident and biologically active GFs (Elkin et al., 2001). Indeed, previous studies have demonstrated that degradation of HS by heparinase enables cell movement through extracellular barriers and releases HS-bound GFs from ECM depots, making them available (Vlodavsky, et al., 1996). The great part of information has been obtained in different *in vitro* and *in vivo* models about FGF which can bind and can be released from HSPGs in the ECM or on the cell surface (Patel et al., 2007; Venero Galanternik et al., 2015). Other information have been reported for the VEGF whose interaction with HS favours the related biological activity, independently of Hep activity (Chan et al., 2020; Beckouche et al., 2015). Furthermore, it is reported that the interaction of HS on EGF is more effective with the heparin-binding epidermal growth factor-like growth factor (HB-EGF) (Higashiyama et al., 1993). Our outcomes surprisingly report very similar features for each GF analysed together with HS, highlighting how this aspect could need a closer look in the future.

Considering that, it is important to underline that the levels of competing GFs and the assessment of their HS-binding properties can influence the binding, activation, and biological response of other GFs, especially when already bind to the heparin-derived structures, although GFs do not share the same receptors. Thus, the cell response to GFs is not only dependent on their concentration in ECM but can be also modulated by the presence of macromolecules differently cleaved (Forsten-Williams et al., 2008). Moreover, in skin wound healing the competitions among the GFs must be addressed in-depth both about the binding on their own receptor and also on HSPGs (Nurkesh et al., 2020). In this case, accurate predictions of GF response within complex *in vivo* environments will require a detailed characterization of the levels of competing growth factors and an appreciation of their HS-binding properties. Here, we have demonstrated that HS + GFs mix is able to promote keratinocytes, fibroblasts and endothelial cells activation, comprising motility, proliferation and differentiation processes in a more marked fashion when associated to Hep too. Moreover, the presence of exogenous heparinase represents the key element for the obtainment of very positive effects in the induction of tissue regeneration if associated to its own substrate behind the mix of GFs. Interestingly, we have also demonstrated that the enzyme alone is not able to act as pro-healing compound, beside its numerous activities (Jin and Zhou, 2017). This could be explained by the necessity to add an exogenous amount of HS, as substrate, due to its limited existence in the injured lesions. On the other hand, the Hep levels still represent an attractive cue for future investigation in the field of skin wound healing. Indeed, it is reported that under physiological condition, its expression is restricted to endothelial cells, keratinocytes and placental trophoblasts (Vreys and David, 2007). During inflammation and immune responses, heparanase is induced in platelets, neutrophils, macrophages and activated lymphocytes (Wu et al., 2015). Therefore, there is an emerging link between the role of heparanase and inflammatory disorders, including in skin section, where, in healthy condition, this enzyme is almost not detected (Goldberg et al., 2013). Moreover, heparanase seems to be involved in cutaneous inflammation, as proved by macrophages activity in specific skin lesions as psioriatic ones (Lerner et al., 2014). Nonetheless, the expression and the function of heparinase in skin wound healing has been not yet investigated in depth. Further assessments are required to solve these issues, particularly focusing on the contest of chronic lesions.

In general, the role of HS is often guaranteed as co-elements of HSPGs, coreceptors in which HS links various members of the GFs family, mainly FGF and VEGF, acting as a cofactor to facilitate the high-affinity receptor binding (Chang et al., 2000). At this regard, HS can bind FGF in a multivalent manner inducing its oligomerization, responsible for FGF receptor dimerization, activation, and signaling (Vlodavsky, et al., 1996). HS may promote the activity of FGF making it capable of simultaneously binding to regions on both the growth factor and its receptor (Venero Galanternik et al., 2015; Chang et al., 2000). Actually, the potential HS action as sequestrator of GFs may be the reason of our surprisingly finding of a significant inversion of all the pro-healing positive effects by HS and GFs mixed together, without Hep compared to single agents alone, both *in vitro* and *in vivo*. Then, following the heparinase-induced degradation of HS, both GFs, as ligands, and HS as binder, are released in the surrounding environment promoting the ECM remodelling and the enhancement of the main cell processes important in the wound healing (Diller and Tabor, 2022). Further investigations could be useful to complete the understanding of the potential role of heparinase enzyme as inhibitor on this kind of sequestration.

Moreover, this specific result could appear in contrast with what we have seen about the pro-repair effects of GFs and HS, taken separately. Indeed, we have confirmed the activity of HS as key participant in cell proliferation, cell migration, collagen fiber formation, basement membrane regeneration, granulation tissue formation, and cell adhesion associated with wound healing (Gallo et al., 2015; Iozzo and Murdoch, 1996; Nasser, 2008). In addition, our data further prove that the use of GFs for skin wound healing management has been described in depth and is notably justified by their well-known powerful effects on multiple spatially and temporally differentiated phases of tissue repair. Therefore, our results highlighted the relevant efficacy of the whole combination in skin wound healing. In detail, to the known important contribution of the single component HS and GFs in cell activation, we have shown that their association, together with the enzyme, contributes to the correct qualitative tissue deposition with the main characteristics of a correct re-epithelialization (Martin, 1997). Nevertheless, extensive biochemical explications need to show the interaction among all the molecules we used in this work.

The therapy of skin wound, including pressure lesions of different degrees, represents an unmet medical need that requires detailed approaches through novel drug delivery systems as polymer gels, nanoparticles-based devices, pre-coated dressings in order to ensure the effectiveness of treatments (Yamakawa and Hayashida, 2019). Lots of these modern devices also require the engagement of ECM-based scaffolds contributing to the direct cell activation and to the release of therapeutic agents to improve the lesions outcome (Da et al., 2021). These advanced approaches could reserve important questions about biocompatibility, biodegradability, hydrophilic features, water adsorption, degradation, drug release from the developed devices.

5. Conclusion

The development of new kinds of topical devices which could maintain features based on user-friendliness and stability, allowing additional pro-healing effects deriving by just one device in full accordance with patient compliance is encouraged. At this regard, we have observed that the combination of HS, GFs and Hep apports an important positive action in the skin repair and each element is able to significantly reinforce the activity of the other ones in the process of in tissue regeneration. These data support, as future perspective, the creation of innovative polymer-based devices containing this association to test *in vivo* and hopefully in patients affected by pressure lesions of different kind and degree.

CRediT authorship contribution statement

Raffaella Belvedere: Investigation, Conceptualization, Methodology, Data curation, Formal analysis, Writing – original draft. **Nunzia Novizio:** Investigation, Methodology. **Mariangela Palazzo:** Methodology. **Emanuela Pessolano:** Investigation, Methodology. **Antonello Petrella:** Conceptualization, Formal analysis, Writing – review & editing, Supervision.

Declaration of competing interest

The authors declare that they have no known competing financial interests or personal relationships that could have appeared to influence the work reported in this paper.

Data availability

Data will be made available on request.

Acknowledgements:

The work conducted in our laboratory and referred to in this paper was funded by University of Salerno (FARB 2020, 2021), and by “Contratto di sviluppo CDS 000463 - Altergon Italia Srl” (CDS_000463).

Appendix A. Supplementary data

Supplementary data to this article can be found online at https://doi.org/10.1016/j.ejphar.2023.176138.

References

Anderegg, U., Halfter, N., Schnabelrauch, M., Hintze, V., 2021. Collagen/glycosaminoglycan-based matrices for controlling skin cell responses. Biol. Chem. 402, 1325–1335. https://doi.org/10.1515/hsz-2021-0176.

Bame, K.J., 2001. Heparanases: endoglycosidases that degrade heparan sulfate proteoglycans. Glycobiology 11, 91R–98R. https://doi.org/10.1093/glycob/11.6.91r.

Beckouche, N., Bignon, M., Lelarge, V., Mathivet, T., Pichol-Thievend, C., Berndt, S., Hardouin, J., Garand, M., Ardidie-Robouant, C., Barret, A., Melino, G., Lortat-Jacob, H., Muller, L., Monnot, C., Germain, S., 2015. The interaction of heparan sulfate proteoglycans with endothelial transglutaminase-2 limits VEGF165-induced angiogenesis. Sci. Signal. 8, ra70. https://doi.org/10.1126/scisignal.aaa0963.

Belvedere, R., Bizzarro, V., Forte, G., Dal Piaz, F., Parente, L., Petrella, A., 2016. Annexin A1 contributes to pancreatic cancer cell phenotype, behaviour and metastatic potential independently of Formyl Peptide Receptor pathway. Sci. Rep. 6, 29660 https://doi.org/10.1038/srep29660.

Belvedere, R., Bizzarro, V., Parente, L., Petrella, F., Petrella, A., 2018a. Effects of Prisma® Skin dermal regeneration device containing glycosaminoglycans on human keratinocytes and fibroblasts. Cell Adhes. Migrat. 12, 168–183. https://doi.org/10.1080/19336918.2017.1340137.

Belvedere, R., Bizzarro, V., Parente, L., Petrella, F., Petrella, A., 2017. The pharmaceutical device Prisma® skin promotes *in vitro* angiogenesis through endothelial to mesenchymal transition during skin wound healing. Int. J. Mol. Sci. 18, 1614. https://doi.org/10.3390/ijms18081614.

Belvedere, R., Bizzarro, V., Popolo, A., Dal Piaz, F., Vasaturo, M., Picard, i P., Parente, L., Petrella, A., 2014. Role of intracellular and extracellular annexin A1 in migration and invasion of human pancreatic carcinoma cells. BMC Cancer 14, 961. https://doi.org/10.1186/1471-2407-14-961.

Belvedere, R., Morretta, E., Pessolano, E., Novizio, N., Tosco, A., Porta, A., Whiteford, J., Perretti, M., Filippelli, A., Monti, M.C., Petrella, A., 2021a. Mesoglycan exerts its fibrinolytic effect through the activation of annexin A2. J. Cell. Physiol. 236, 4926–4943. https://doi.org/10.1002/jcp.30207.

Belvedere, R., Novizio, N., Morello, S., Petrella, A., 2022. The combination of mesoglycan and VEGF promotes skin wound repair by enhancing the activation of endothelial cells and fibroblasts and their cross-talk. Sci. Rep. 12, 11041 https://doi.org/10.1038/s41598-022-15227-1.

Belvedere, R., Novizio, N., Pessolano, E., Tosco, A., Eletto, D., Porta, A., Campiglia, P., Perretti, M., Filippelli, A., Petrella, A., 2020a. Heparan sulfate binds the extracellular Annexin A1 and blocks its effects on pancreatic cancer cells. Biochem. Pharmacol. 182, 114252 https://doi.org/10.1016/j.bcp.2020.114252.

Belvedere, R., Pessolano, E., Novizio, N., Tosco, A., Eletto, D., Porta, A., Filippelli, A., Petrella, F., Petrella, A., 2021b. The promising pro-healing role of the association of mesoglycan and lactoferrin on skin lesions. Eur. J. Pharmaceut. Sci. 163, 105886 https://doi.org/10.1016/j.ejps.2021.105886.

Belvedere, R., Pessolano, E., Porta, A., Tosco, A., Parente, L., Petrella, F., Perretti, M., Petrella, A., 2020b. Mesoglycan induces the secretion of microvesicles by keratinocytes able to activate human fibroblasts and endothelial cells: a novel mechanism in skin wound healing. Eur. J. Pharmacol. 869, 172894 https://doi.org/10.1016/j.ejphar.2019.172894.

Belvedere, R., Saggese, P., Pessolano, E., Memoli, D., Bizzarro, V., Rizzo, F., Parente, L., Weisz, A., Petrella, A., 2018b. miR-196a is able to restore the aggressive phenotype of annexin A1 knock-out in pancreatic cancer cells by CRISPR/Cas9 genome editing. Int. J. Mol. Sci. 19 (1967) https://doi.org/10.3390/ijms19071967.

Bizzarro, V., Belvedere, R., Migliaro, V., Romano, E., Parente, L., Petrella, A., 2017. Hypoxia regulates ANXA1 expression to support prostate cancer cell invasion and aggressiveness. Cell Adhes. Migrat. 1, 247–260. https://doi.org/10.1080/19336918.2016.1259056.

Bizzarro, V., Belvedere, R., Pessolano, E., Parente, L., Petrella, F., Perretti, M., Petrella, A., 2019. Mesoglycan induces keratinocyte activation by triggering syndecan-4 pathway and the formation of the annexin A1/S100A11 complex. J. Cell. Physiol. 234, 20174–20192. https://doi.org/10.1002/jcp.28618.

Boyce, A., Walsh, G., 2022. Production, characteristics and applications of microbial heparinases. Biochimie 198, 109–140. https://doi.org/10.1016/j.biochi.2022.03.011.

Cerezo-Magaña, M., Christianson, H.C., van Kuppevelt, T.H., Forsberg-Nilsson, K., Belting, M., 2021. Hypoxic induction of exosome uptake through proteoglycan-dependent endocytosis fuels the lipid droplet phenotype in glioma. Mol. Cancer Res. 19, 528–540. https://doi.org/10.1158/1541-7786.MCR-20-0560.

Chan, S.J., Esposito, E., Hayakawa, K., Mandaville, E., Smith, R.A.A., Guo, S., Niu, W., Wong, P.T., Cool, S.M., Lo, E.H., Nurcombe, V., 2020. Vascular endothelial growth factor 165-binding heparan sulfate promotes functional recovery from cerebral ischemia. Stroke 51, 2844–2853. https://doi.org/10.1161/STROKEAHA.119.025304.

Chang, Z., Meyer, K., Rapraeger, A.C., Friedl, A., 2000. Differential ability of heparan sulfate proteoglycans to assemble the fibroblast growth factor receptor complex in situ. FASEB J. 14, 137–144. https://doi.org/10.1096/fasebj.14.1.137.

Chappell, D., Jacob, M., Rehm, M., Stoeckelhuber, M., Welsch, U., Conzen, P., Becker, B. F., 2008. Heparinase selectively sheds heparan sulphate from the endothelial glycocalyx. Biol. Chem. 389, 79–82. https://doi.org/10.1515/BC.2008.005.

Chen, F., Shen, Y., Mohanasundaram, P., Lindström, M., Ivaska, J., Ny, T., Eriksson, J.E., 2016. Vimentin coordinates fibroblast proliferation and keratinocyte differentiation in wound healing via TGF-β-Slug signaling. Proc. Natl. Acad. Sci. U.S.A. 113, E4320–E4327. https://doi.org/10.1073/pnas.1519197113.

Corti, F., Wang, Y., Rhodes, J.M., Atri, D., Archer-Hartmann, S., Zhang, J., Zhuang, Z.W., Chen, D., Wang, T., Wang, Z., Azadi, P., Simons, M., 2019. N-terminal syndecan-2 domain selectively enhances 6-O heparan sulfate chains sulfation and promotes VEGFA165-dependent neovascularization. Nat. Commun. 10 (2019), 1562. https://doi.org/10.1038/s41467-019-09605-z. Erratum in: Nat Commun. 10, 2124.

Da, L.C., Huang, Y.Z., Xie, H.Q., Zheng, B.H., Huang, Y.C., Du, S.R., 2021. Membranous extracellular matrix-based scaffolds for skin wound healing. Pharmaceutics 13, 1796. https://doi.org/10.3390/pharmaceutics13111796.

Dejana, E., Hirschi, K.K., Simons, M., 2017. The molecular basis of endothelial cell plasticity. Nat. Commun. 8, 14361 https://doi.org/10.1038/ncomms14361.

Diller, R.B., Tabor, A.J., 2022. The role of the extracellular matrix (ECM) in wound healing: a review. Biomimetics 7, 87. https://doi.org/10.3390/biomimetics7030087.

Ding, Z., Wang, X., Khaidakov, M., Liu, S., Dai, Y., Mehta, J.L., 2012. Degradation of heparan sulfate proteoglycans enhances oxidized-LDL-mediated autophagy and apoptosis in human endothelial cells. Biochem. Biophys. Res. Commun. 426, 106–111. https://doi.org/10.1016/j.bbrc.2012.08.044.

Dong, W., Lu, W., McKeehan, W.L., Luo, Y., Ye, S., 2012. Structural basis of heparan sulfate-specific degradation by heparinase III. Protein Cell 3, 950–961. https://doi.org/10.1007/s13238-012-2056-z.

Elkin, M., Ilan, N., Ishai-Michaeli, R., Friedmann, Y., Papo, O., Pecker, I., Vlodavsky, I., 2001. Heparanase as mediator of angiogenesis: mode of action. FASEB J. 15, 1661–1663. https://doi.org/10.1096/fj.00-0895fje.

Esko, J.D., Lindahl, U., 2001. Molecular diversity of heparan sulfate. J. Clin. Invest. 108, 169–173. https://doi.org/10.1172/JCI13530.

Festa, M., Petrella, A., Alfano, S., Parente, L., 2009. R-roscovitine sensitizes anaplastic thyroid carcinoma cells to TRAIL-induced apoptosis via regulation of IKK/NF-kappaB pathway. Int. J. Cancer 124, 2728–2736. https://doi.org/10.1002/ijc.24260.

Forsten-Williams, K., Chu, C.L., Fannon, M., Buczek-Thomas, J.A., Nugent, M.A., 2008. Control of growth factor networks by heparan sulfate proteoglycans. Ann. Biomed. Eng. 36, 2134–2148. https://doi.org/10.1007/s10439-008-9575-z.

Franco, P., Belvedere, R., Pessolano, E., Liparoti, S., Pantani, R., Petrella, A., De Marco, I., 2019. PCL/Mesoglycan devices obtained by supercritical foaming and impregnation. Pharmaceutics 11, 631. https://doi.org/10.3390/pharmaceutics11120631.

Franco, P., Pessolano, E., Belvedere, R., Petrella, A., De Marco, I., 2020. Supercritical impregnation of mesoglycan into calcium alginate aerogel for wound healing. J. Supercrit. Fluids 157, 104711. https://doi.org/10.1016/j.supflu.2019.104711.

Freedman, B.R., Hwang, C., Talbot, S., Hibler, B., Matoori, S., Mooney, D.J., 2023. Breakthrough treatments for accelerated wound healing. Sci. Adv. 9, eade7007 https://doi.org/10.1126/sciadv.ade7007.

Gallo, R.L., Bucay, V.W., Shamban, A.T., Lima-Maribona, J., Lewis, A.B., Ditre, C.M., Mayoral, F.A., Gold, M.H., 2015. The potential role of topically applied heparan sulfate in the treatment of photodamage. J. Drugs Dermatol. 14, 669–674.

Goldberg, R., Meirovitz, A., Hirshoren, N., Bulvik, R., Binder, A., Rubinstein, A.M., Elkin, M., 2013. Versatile role of heparanase in inflammation. Matrix Biol. 32, 234–240. https://doi.org/10.1016/j.matbio.2013.02.008.

Halbleib, J.M., Nelson, W.J., 2006. Cadherins in development: cell adhesion, sorting, and tissue morphogenesis. Genes Dev. 20, 3199–3214. https://doi.org/10.1101/gad.1486806.

Han, G., Ceilley, R., 2017. Chronic wound healing: a review of current management and treatments. Adv. Ther. 34, 599–610. https://doi.org/10.1007/s12325-017-0478-y.

Higashiyama, S., Abraham, J.A., Klagsbrun, M., 1993. Heparin-binding EGF-like growth factor stimulation of smooth muscle cell migration: dependence on interactions with cell surface heparan sulfate. J. Cell Biol. 122, 933–940. https://doi.org/10.1083/jcb.122.4.933.

Hoogewerf, A.J., Leone, J.W., Reardon, I.M., Howe, W.J., Asa, D., Heinrikson, R.L., Ledbetter, S.R., 1995. CXC chemokines connective tissue activating peptide-III and neutrophil activating peptide-2 are heparin/heparan sulfate-degrading enzymes. J. Biol. Chem. 270, 3268–3277. https://doi.org/10.1074/jbc.270.7.3268.

Iozzo, R.V., Murdoch, A.D., 1996. Proteoglycans of the extracellular environment: clues from the gene and protein side offer novel perspectives in molecular diversity and function. FASEB J. 10, 598–614.

Januszyk, M., Kwon, S.H., Wong, V.W., Padmanabhan, J., Maan, Z.N., Whittam, A.J., Major, M.R., Gurtner, G.C., 2017. The role of focal adhesion Kinase in keratinocyte fibrogenic gene expression. Int. J. Mol. Sci. 18, 1915. https://doi.org/10.3390/ijms18091915.

Jin, H., Zhou, S., 2017. The functions of heparanase in human diseases. Mini Rev. Med. Chem. 17, 541–548. https://doi.org/10.2174/1389557516666161101143643.

Jones, A.L., Hulett, M.D., Parish, C.R., 2004. Histidine-rich glycoprotein binds to cell-surface heparan sulfate via its N-terminal domain following Zn^{2+} chelation. J. Biol. Chem. 279, 30114–30122. https://doi.org/10.1074/jbc.M401996200.

Lerner, I., Zcharia, E., Neuman, T., Hermano, E., Rubinstein, A.M., Vlodavsky, I., Elkin, M., 2014. Heparanase is preferentially expressed in human psoriatic lesions and induces development of psoriasiform skin inflammation in mice. Cell. Mol. Life Sci. 71, 2347–2357. https://doi.org/10.1007/s00018-013-1496-9.

Martin, P., 1997. Wound healing–aiming for perfect skin regeneration. Science 276, 75–81. https://doi.org/10.1126/science.276.5309.75.

Masola, V., Bellin, G., Gambaro, G., Onisto, M., 2018. Heparanase: a multitasking protein involved in extracellular matrix (ECM) remodeling and intracellular events. Cells 7, 236. https://doi.org/10.3390/cells7120236.

Matsuo, I., Kimura-Yoshida, C., 2014. Extracellular distribution of diffusible growth factors controlled by heparan sulfate proteoglycans during mammalian embryogenesis. Philos. Trans. R. Soc. Lond. B Biol. Sci. 369, 20130545 https://doi.org/10.1098/rstb.2013.0545.

Meier, N.T., Haslam, I.S., Pattwell, D.M., Zhang, G.Y., Emelianov, V., Paredes, R., Debus, S., Augustin, M., Funk, W., Amaya, E., Kloepper, J.E., Hardman, M.J., Paus, R., 2013. Thyrotropin-releasing hormone (TRH) promotes wound re-

epithelialisation in frog and human skin. PLoS One 8, e73596. https://doi.org/10.1371/journal.pone.0073596.
Nasser, N.J., 2008. Heparanase involvement in physiology and disease. Cell. Mol. Life Sci. 65, 1706–1715. https://doi.org/10.1007/s00018-008-7584-6.
Novizio, N., Belvedere, R., Pessolano, E., Morello, S., Tosco, A., Campiglia, P., Filippelli, A., Petrella, A., 2021. ANXA1 contained in EVs regulates macrophage polarization in tumor microenvironment and promotes pancreatic cancer progression and metastasis. Int. J. Mol. Sci. 22, 11018 https://doi.org/10.3390/ijms222011018.
Novizio, N., Belvedere, R., Pessolano, E., Tosco, A., Porta, A., Perretti, M., Campiglia, P., Filippelli, A., Petrella, A., 2020. Annexin A1 released in extracellular vesicles by pancreatic cancer cells activates components of the tumor microenvironment, through interaction with the formyl-peptide receptors. Cells 9, 2719. https://doi.org/10.3390/cells9122719.
Nurkesh, A., Jaguparov, A., Jimi, S., Saparov, A., 2020. Recent advances in the controlled release of growth factors and cytokines for improving cutaneous wound healing. Front. Cell Dev. Biol. 8, 638. https://doi.org/10.3389/fcell.2020.00638.
Olczyk, P., Mencner, Ł., Komosinska-Vassev, K., 2015. Diverse roles of heparan sulfate and heparin in wound repair. BioMed Res. Int. 2015, 549417 https://doi.org/10.1155/2015/549417.
Park, H., Kim, M., Kim, H.J., Lee, Y., Seo, Y., Pham, C.D., Lee, J., Byun, S.J., Kwon, M.H., 2017. Heparan sulfate proteoglycans (HSPGs) and chondroitin sulfate proteoglycans (CSPGs) function as endocytic receptors for an internalizing anti-nucleic acid antibody. Sci. Rep. 7, 14373 https://doi.org/10.1038/s41598-017-14793-z.
Park, J.W., Hwang, S.R., Yoon, I.S., 2017. Advanced growth factor delivery systems in wound management and skin regeneration. Molecules 22, 1259. https://doi.org/10.3390/molecules22081259.
Patel, V.N., Knox, S.M., Likar, K.M., Lathrop, C.A., Hossain, R., Eftekhari, S., Whitelock, J.M., Elkin, M., Vlodavsky, I., Hoffman, M.P., 2007. Heparanase cleavage of perlecan heparan sulfate modulates FGF10 activity during ex vivo submandibular gland branching morphogenesis. Development 134, 4177–4186. https://doi.org/10.1242/dev.011171.
Pessolano, E., Belvedere, R., Novizio, N., Filippelli, A., Perretti, M., Whiteford, J., Petrella, A., 2021. Mesoglycan connects Syndecan-4 and VEGFR2 through Annexin A1 and formyl peptide receptors to promote angiogenesis *in vitro*. FEBS J. 288, 6428–6446. https://doi.org/10.1111/febs.16043.
Petrella, F., Belvedere, R., Labbro, V., Apicella, A., Bizzarro, V., Pessolano, E., Parente, L., Petrella, A., 2020. A new pharmaceutical device containing mesoglycan modulates fibroblasts function *in vivo*. Pharmacologyonline 1, 20–30.
Venero Galanternik, M., Kramer, K.L., Piotrowski, T., 2015. Heparan sulfate proteoglycans regulate fgf signaling and cell polarity during collective cell migration. Cell Rep. 10, 414–428. https://doi.org/10.1016/j.celrep.2014.12.043.
Vlodavsky, I., Miao, H.Q., Medalion, B., Danagher, P., Ron, D., 1996. Involvement of heparan sulfate and related molecules in sequestration and growth promoting activity of fibroblast growth factor. Cancer Metastasis Rev. 15, 177–186. https://doi.org/10.1007/BF00437470.
Vreys, V., David, G., 2007. Mammalian heparanase: what is the message? J. Cell Mol. Med. 11, 427–452. https://doi.org/10.1111/j.1582-4934.2007.00039.x.
Wang, X., Ge, J., Tredget, E.E., Wu, Y., 2013. The mouse excisional wound splinting model, including applications for stem cell transplantation. Nat. Protoc. 8, 302–309. https://doi.org/10.1038/nprot.2013.002.
Wu, C.Y., Asano, Y., Taniguchi, T., Sato, S., Yu, H.S., 2015. Serum heparanase levels: a protective marker against digital ulcers in patients with systemic sclerosis. J. Dermatol. 42, 625–628. https://doi.org/10.1111/1346-8138.12842.
Yamakawa, S., Hayashida, K., 2019. Advances in surgical applications of growth factors for wound healing. Burns Trauma 7, 10. https://doi.org/10.1186/s41038-019-0148-1.
Yan, D., Lin, X., 2009. Shaping morphogen gradients by proteoglycans. Cold Spring Harbor Perspect. Biol. 1, a002493. https://doi.org/10.1101/cshperspect.a002493.
Yan, L., Cao, R., Liu, Y., Wang, L., Pan, B., Lv, X., Jiao, H., Zhuang, Q., Sun, X., Xiao, R., 2016. MiR-21-5p links epithelial-mesenchymal transition phenotype with stem-like cell signatures via AKT signaling in keloid keratinocytes. Sci. Rep. 6, 28281 https://doi.org/10.1038/srep28281.
Zcharia, E., Zilka, R., Yaar, A., Yacoby-Zeevi, O., Zetser, A., Metzger, S., Sarid, R., Naggi, A., Casu, B., Ilan, N., Vlodavsky, I., Abramovitch, R., 2005. Heparanase accelerates wound angiogenesis and wound healing in mouse and rat models. FASEB J. 19, 211–221. https://doi.org/10.1096/fj.04-1970com.
Zeng, Y., Ebong, E.E., Fu, B.M., Tarbell, J.M., 2012. The structural stability of the endothelial glycocalyx after enzymatic removal of glycosaminoglycans. PLoS One 7, e43168. https://doi.org/10.1371/journal.pone.0043168.